

Scattering of a weakly bound dimer from a hard wall in one dimension

Xican Zhang^{1,2} and Shina Tan^{1,2,*}

¹*International Center for Quantum Materials, Peking University, Beijing 100871, China*

²*Beijing Key Laboratory of Quantum Devices, Peking University, Beijing 100871, China*

(Dated: March 17, 2026)

We consider a dimer formed by two particles with an attractive contact interaction in one dimension, colliding with a hard wall. We compute the scattering phase shifts and the reflection coefficients for various collision energies and various mass ratios of the two particles. For low-energy collisions (with dimer kinetic energies much smaller than the binding energy) our results are consistent with those of D. Lee and M. Pine, *The European Physical Journal A* **47**, 41 (2011). For mass ratios much greater than 1 we use the Born-Oppenheimer approximation to show that the scattering length and the effective range of the dimer-wall collision both depend logarithmically on the mass ratio. For collision energies much greater than the binding energy, the dissociation probability is inversely proportional to the square of the incident momentum of the dimer and we find the constant of proportionality analytically, and we use a semiclassical analysis to approximately derive the “angular distribution” of the dissociated pair, where the “angle” θ depends on the ratio of the velocities of the two outgoing unbound particles.

I. INTRODUCTION

The scattering of quantum particles from hard walls provides a fundamental paradigm for understanding boundary effects. In cold atom experiments, confined systems with tunable interactions can be created in tightly focused optical lattices [1, 2]. An additional laser may be focused to produce a sharp repulsive boundary [3, 4]. Box traps can also be realized for ultracold atoms [5–9], and few-body system in box traps have been studied [10–12]. The emergence of optical tweezer arrays enables the manipulation of individual molecules, such as the CaF molecule [13, 14] and the NaCs molecule [15, 16]. People have studied the collisions between one dimensional (1D) composite objects and obstacles [4, 17–19]. The mass ratio between the constituent particles and the kinetic energy of the collision play important roles in the collision process.

Recent experimental progress has enabled the preparation of ultracold heteronuclear molecules with a wide range of mass ratios [20]. For example, mixtures of ⁴⁰K and ⁶Li reach a mass ratio of approximately 6.7 [21–23], while combinations involving heavier fermionic isotopes such as ¹⁷³Yb with ⁶Li yield mass ratios up to ≈ 29 [24, 25]. Mass ratios exceeding these values are not currently achievable with stable atomic species. However, extreme mass ratios could be reached by tuning effective masses in optical lattices [26].

In this paper, we investigate the scattering of a weakly bound dimer from a hard wall in one dimension. The dimer is formed by two distinguishable particles with masses m_1 and m_2 and with a short-range attractive interaction characterized by a δ -function potential. We focus on two distinct scattering regimes: the low-energy regime, where the dimer reflects elastically, and the inelastic regime above the dissociation threshold, where the

collision can break the dimer into its constituent particles.

Model– Let the coordinates of the two particles with masses m_1 and m_2 be x_1 and x_2 respectively. We assume that the particles interact with a delta function potential and that there is a hard wall at $x = 0$. The two-body wave function $\Psi(x_1, x_2)$ for the energy eigenstate with energy E satisfies the Schrödinger equation

$$\left[-\frac{1}{2m_1} \frac{\partial^2}{\partial x_1^2} - \frac{1}{2m_2} \frac{\partial^2}{\partial x_2^2} + g\delta(x_1 - x_2) \right] \Psi = E\Psi \quad (1)$$

at $x_1, x_2 > 0$, where we set $\hbar = 1$, and the interaction strength $g = -1/\mu a < 0$ corresponds to an attractive interaction, a is the one-dimensional s -wave scattering length between the particles, and $\mu = m_1 m_2 / (m_1 + m_2)$ is the reduced mass. A hard wall is introduced at the origin by imposing the Dirichlet boundary conditions:

$$\Psi(0, x_2) = \Psi(x_1, 0) = 0. \quad (2)$$

The energy E may be expressed as

$$E = \frac{K^2}{2M} - \frac{1}{2\mu a^2}, \quad (3)$$

where K is the magnitude of the center-of-mass incident momentum, $M = m_1 + m_2$ is the total mass of the dimer, and the second term on the right hand side of the above equation is the energy of the bound state in its rest frame. If we solve Eq. (3) at $E = 0$, we get a dissociation threshold momentum

$$K_{\text{th}} = \frac{m_1 + m_2}{\sqrt{m_1 m_2}} \frac{1}{a}. \quad (4)$$

We define the center-of-mass coordinate

$$X = \frac{m_1 x_1 + m_2 x_2}{m_1 + m_2} \quad (5)$$

* shinatan@pku.edu.cn

and the relative coordinate

$$r = x_2 - x_1. \quad (6)$$

For the dimer-wall collision, the wave function takes the following form at $X \rightarrow \infty$:

$$\Psi(x_1, x_2) = e^{-|r|/a} [e^{-iKX} + f e^{iKX}] + \psi_d(x_1, x_2), \quad (7)$$

where f is the amplitude of the reflected wave, and $\psi_d(x_1, x_2)$ denotes the dissociated (unbound) part of the wave function which goes to zero at $X \rightarrow \infty$. The reflection coefficient is

$$R = |f|^2. \quad (8)$$

If $K < K_{\text{th}}$, the dimer scatters elastically off the hard wall, so that the reflection coefficient $R = 1$ and the dissociation component $\psi_d(x_1, x_2)$ decays exponentially at $X \rightarrow \infty$. In this case, the wave function far from the wall reduces to a standing wave $\propto e^{-|r|/a} \sin(KX + \delta)$, where

$$\delta = \frac{1}{2} \arg(-f) \quad (9)$$

is the scattering phase shift. Here $\arg(z)$ means the argument of the complex number z . If $K \ll K_{\text{th}}$ we have the effective range expansion,

$$K \cot \delta = -\frac{1}{a_R} + \frac{1}{2} r_R K^2 + \dots, \quad (10)$$

where a_R is the dimer-wall scattering length, and r_R is the dimer-wall effective range. If $K > K_{\text{th}}$, the incident dimer may dissociate after the collision, so that the reflection coefficient $R < 1$. In this inelastic regime, the scattering phase shift δ is no longer defined in the standard sense. We extend the definition of the scattering phase shift to this regime by still using Eq. (9).

We solve our model with a combination of analytical and numerical methods. Without loss of generality we assume that $m_1 \geq m_2$ from now on. In Sec. II we derive exact solutions using the Bethe Ansatz for the special integrable cases of $m_1/m_2 = 1$ [27] and $m_1/m_2 = 3$ [12]. In Sec. III we derive an integral equation for the problem for arbitrary mass ratios, and solve it numerically. In Sec. IV, for large mass imbalance ($m_1 \gg m_2$), we employ the Born-Oppenheimer approximation to obtain analytical asymptotic results for a_R and r_R . In Sec. V, for high-energy collisions with incident kinetic energies much larger than the binding energy of the dimer, we perform a semi-classical analysis and verify the validity of this analysis by comparing its predictions with those based on the numerical solutions in Sec. III.

II. INTEGRABLE CASES

Integrable systems are known to preserve chemical composition during scattering processes, even when the incident energy exceeds the dissociation threshold [28, 29]. The model introduced in Sec. I is integrable if the mass ratio m_1/m_2 is 1 or 3. The case $m_1/m_2 = 1$ was solved by Bethe ansatz by Gaudin [27]. The ansatz for the mass ratio $m_1/m_2 = 3$ is based on a finite superposition of plane waves associated with a dihedral group D_6 as revealed in [12]. This emergent symmetry is an example of the kinematic symmetries that arise in the “no-tunneling” limit imposed by an impenetrable barrier (the hard wall) as discussed in [30, 31].

If $m_1/m_2 = 1$, the two-body wave function for the dimer colliding with the hard wall is

$$\Psi(x_1, x_2) = e^{-\frac{|x_2 - x_1|}{a}} \sin\left(K \frac{x_1 + x_2}{2} + \delta\right) - e^{-\frac{x_1 + x_2}{a}} \sin\left(K \frac{|x_1 - x_2|}{2} + \delta\right), \quad (11)$$

and the scattering phase shift δ satisfies [4, 19]

$$K \cot \delta = -\frac{2}{a}. \quad (12)$$

Comparing Eq. (12) with Eq. (10), one obtains $a_R = \frac{a}{2}$ [4] and $r_R = 0$ [4].

If $m_1/m_2 = 3$, setting $(k_1, k_2) = (-\frac{3}{4}K + \frac{i}{a}, -\frac{1}{4}K - \frac{i}{a})$ and choosing the coefficients $A_{j\pm}$ in Eq. (18) in Ref. [12] to satisfy appropriate boundary conditions, we get the following exact wave function:

$$\begin{aligned} \Psi(x_1, x_2) = & e^{-\frac{|x_1 - x_2|}{a}} \sin\left(K \frac{3x_1 + x_2}{4} + \delta\right) \\ & - e^{-\frac{x_1 + x_2}{a}} \sin\left[K \frac{3x_1 - x_2}{4} \text{sgn}(x_1 - x_2) + \delta\right] \\ & + \frac{8}{\sqrt{16 + 9a^2K^2}} e^{-\frac{2x_1}{a}} \sin\left(\frac{Kx_2}{2}\right) \theta(x_1 - x_2), \end{aligned} \quad (13)$$

where $\text{sgn}(x)$ is the sign function (defined to be 1 for $x > 0$ and -1 for $x < 0$), $\theta(x)$ is the Heaviside step function, and the scattering phase shift δ satisfies

$$K \cot \delta = -\frac{4}{3a}. \quad (14)$$

Comparing Eq. (14) with Eq. (10), we get $a_R = \frac{3}{4}a$ and $r_R = 0$.

Equations (11) and (13) are valid for all $K > 0$, and thus the reflection coefficient $R = 1$ for all K (even if $K > K_{\text{th}}$) if m_1/m_2 is equal to 1 or 3.

III. GENERAL CASES

We begin by rewriting Eq. (1) in a more convenient form,

$$\left(\frac{\partial^2}{\partial y_1^2} + \frac{\partial^2}{\partial y_2^2} + 2m_1 E\right)\Psi = -\frac{2(1+\beta^2)}{a}\delta(y_1 - \beta y_2)\Psi, \quad (15)$$

where we have introduced the rescaled coordinates,

$$y_1 = x_1, \quad y_2 = \frac{x_2}{\beta}, \quad \text{with} \quad \beta = \sqrt{\frac{m_1}{m_2}}. \quad (16)$$

Let $G(y_1, y_2, y'_1, y'_2)$ be the Green's function for the non-interacting problem with hard-wall boundary conditions, satisfying

$$\left(\frac{\partial^2}{\partial y_1^2} + \frac{\partial^2}{\partial y_2^2} + 2m_1 E\right)G = \delta(y_1 - y'_1)\delta(y_2 - y'_2), \quad (17)$$

with $G = 0$ whenever $y_1 = 0$, $y_2 = 0$, $y'_1 = 0$ or $y'_2 = 0$. This Green's function can be constructed via the method of images:

$$\begin{aligned} G(y_1, y_2, y'_1, y'_2) = & G_0\left(\sqrt{(y_1 - y'_1)^2 + (y_2 - y'_2)^2}\right) \\ & + G_0\left(\sqrt{(y_1 + y'_1)^2 + (y_2 + y'_2)^2}\right) \\ & - G_0\left(\sqrt{(y_1 - y'_1)^2 + (y_2 + y'_2)^2}\right) \\ & - G_0\left(\sqrt{(y_1 + y'_1)^2 + (y_2 - y'_2)^2}\right), \end{aligned} \quad (18)$$

and

$$G_0(r) = \begin{cases} -\frac{1}{2\pi}K_0(\sqrt{-2m_1 E}r), & E < 0 \\ \frac{1}{2\pi}\ln r, & E = 0 \\ -\frac{i}{4}H_0^{(1)}(\sqrt{2m_1 E}r), & E > 0 \end{cases}. \quad (19)$$

Here $K_0(\xi)$ is the decaying Bessel function, and $H_0^{(1)}(\xi)$ is the Hankel function of the first kind. Using the Green's function method, the wave function in scaled coordinates satisfies the Lippmann-Schwinger equation

$$\Psi(\mathbf{y}) = -\frac{2(1+\beta^2)}{a}\iint d^2\mathbf{y}'G(\mathbf{y}, \mathbf{y}')\delta(y'_1 - \beta y'_2)\Psi(\mathbf{y}'), \quad (20)$$

where $\mathbf{y} = (y_1, y_2)$, $\mathbf{y}' = (y'_1, y'_2)$, and the integral runs over the first quadrant, $y'_1, y'_2 > 0$. Transforming back to the original coordinates (x_1, x_2) , we obtain

$$\Psi(x_1, x_2) = -\frac{2(1+\beta^2)}{a\beta}\int_0^\infty G(x_1, x_2/\beta, z, z/\beta)\psi(z)dz, \quad (21)$$

where $\psi(z) \equiv \Psi(z, z)$. Setting $x_1 = x_2 = x$ in Eq. (21) yields a closed integral equation for $\psi(x)$:

$$\psi(x) = -\frac{2(1+\beta^2)}{a\beta}\int_0^\infty G(x, x/\beta, z, z/\beta)\psi(z)dz. \quad (22)$$

According to Eq. (7), at $x \rightarrow \infty$ we have

$$\psi(x) = e^{-iKx} + f e^{iKx} + \psi_d(x), \quad (23)$$

where $\psi_d(x) \equiv \psi_d(x, x)$ goes to zero at $x \rightarrow \infty$.

If $E > 0$, there is usually a nonzero probability D for the dimer to dissociate after collision with the wall. For any fixed ratio $x_2/x_1 \neq 1$, we expand Ψ in Eq. (21) when x_1 and x_2 go to infinity simultaneously, and find that

$$\Psi(x_1, x_2) = c(\theta)\rho^{-1/2}e^{iQ\rho} + o(\rho^{-1/2}), \quad (24)$$

where $Q = \sqrt{2ME}$,

$$\rho = \sqrt{\frac{m_1 x_1^2 + m_2 x_2^2}{m_1 + m_2}}, \quad (25)$$

$$\theta = \arctan\left(\sqrt{\frac{m_2}{m_1}}\frac{x_2}{x_1}\right), \quad (26)$$

$$\begin{aligned} c(\theta) = e^{i\frac{\pi}{4}}\frac{\sqrt{2}K_{\text{th}}}{\sqrt{\pi}Q}\int_0^\infty \{ \cos[Qz \cos(\theta - \theta_0)] \\ - \cos[Qz \cos(\theta + \theta_0)] \} \psi(z)dz, \end{aligned} \quad (27)$$

and

$$\theta_0 = \arctan\sqrt{m_2/m_1}. \quad (28)$$

By studying the probability flux, we find that the probability that the two particles dissociate and end up in the infinitesimal range $(\theta, \theta + d\theta)$ at large ρ is $P(\theta)d\theta$ and

$$P(\theta) = \frac{QK_{\text{th}}}{K}|c(\theta)|^2. \quad (29)$$

The total dissociation probability is

$$D = \int_0^{\pi/2} P(\theta)d\theta. \quad (30)$$

One can analytically show that $R + D = 1$.

We have solved Eq. (22) numerically to determine f for various mass ratios and incident momenta. We then computed the reflection coefficient R and the scattering phase shift δ , using Eqs. (8) and (9). For negative energies ($K < K_{\text{th}}$), the scattering is purely elastic and is fully characterized by the scattering phase shift δ . For positive energies ($K > K_{\text{th}}$), the scattering is inelastic (unless m_1/m_2 equals 1 or 3), and the reflection coefficient $R < 1$ (unless m_1/m_2 is 1 or 3). In Fig. 1 we plot the scattering phase shift δ versus K/K_{th} for var-

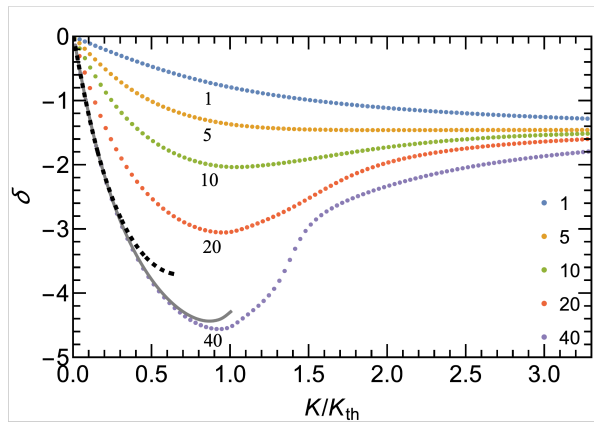


FIG. 1. Dotted curves: the dimer-wall scattering phase shift δ versus K/K_{th} for mass ratios 1, 5, 10, 20, and 40. The numbers below the dotted curves are the corresponding mass ratios. Dashed curve: the prediction of Eq. (35) based on an approximate treatment of the Born-Oppenheimer approximation for the mass ratio $m_1/m_2 = 40$. Grey curve: the prediction of the Born-Oppenheimer approximation, based on the numerical solutions of Eq. (32) together with Eqs. (31) and (33) for $m_1/m_2 = 40$.

ious mass ratios. The minimum of δ exhibits a strong dependence on the mass ratio m_1/m_2 . For larger values of the mass ratio, δ decreases more rapidly as K increases initially. In Fig. 1 we also show the approximate results for the phase shifts for a large mass ratio, $m_1/m_2 = 40$, using the Born-Oppenheimer approximation discussed in Sec. IV. δ approaches $-\pi/2$ as $K \rightarrow \infty$ for any mass ratio.

We also extracted the dimer-wall scattering length a_R and effective range r_R from the scattering phase shifts at low incident momenta ($K \ll K_{\text{th}}$) and plotted the results versus $\ln(m_1/m_2)$ in Fig. 2. Notably, as analytically confirmed by Eqs. (12) and (14), the dimer-wall scattering length a_R is $a/2$ for the mass ratio $m_1/m_2 = 1$ and $3a/4$ for $m_1/m_2 = 3$, and the effective range r_e vanishes for $m_1/m_2 = 1$ and for $m_1/m_2 = 3$. The curves for a_R and r_R approach straight lines at large $\ln(m_1/m_2)$ in Fig. 2, and we explain this finding using the Born-Oppenheimer approximation in Sec. IV.

When the incident kinetic energy of the dimer exceeds its binding energy, such that $K > K_{\text{th}}$, the collision of the dimer with the wall could break up the dimer. We numerically solved Eq. (22) and determined the reflection coefficient $R = |f|^2$ for various values of the incident momentum and the mass ratio.

We plot R versus K/K_{th} in Fig. 3 for mass ratios ranging from 1 to 10, and in Fig. 4 for large mass ratios 20, 40, 75.8, and 140. Notably, for mass ratios 1 and 3, the reflection coefficient remains equal to one for all collision energies, indicating full reflection without dissociation, and this is a consequence of integrability discussed in Sec. II. For other mass ratios, R generally first decreases as the collision energy increases, and then increases as

the collision energy further increases. Furthermore, systems with larger mass ratios demonstrate a more profound suppression of R for appropriate energies, revealing the effect of mass imbalance on the inelastic scattering process. In Fig. 5 we plot the minimum value of the reflection coefficient, R_{min} , for different mass ratios. The two insets in Fig. 5 show the moderate mass ratio regime $1 \leq m_1/m_2 \leq 4.3$ and the regime where R_{min} is close to zero, respectively. In the moderate mass ratio regime, R remains close to unity, while a significant mass imbalance substantially enhances the probability of dissociation. And we find that R_{min} can reach zero at a critical mass ratio of about 75.8 (at $K/K_{\text{th}} \approx 1.24$ as shown in Fig. 4). As the incident momentum goes to infinity, the reflection coefficient eventually approaches unity. This effect can be analytically understood as arising from the asymptotic scaling $R = 1 - O(1/K^2)$, which we will derive in Sec. V.

If the collision breaks up the dimer, the dissociated pair may move along different “directions” on the (x_1, x_2) plane. The “direction” is characterized by the “angle” θ defined in Eq. (26), and in Fig. 6 we plot the “angular distribution” $P(\theta)$ for mass ratios 2 and 4 at several incident momenta. At larger and larger incident momenta, the angular distribution becomes a narrower and narrower peak centered around a particular “angle” θ_c whose value depends on the mass ratio. In Sec. V we shall derive this feature using a semiclassical analysis.

IV. BORN-OPPENHEIMER APPROXIMATION

For large mass ratios ($m_1/m_2 \gg 1$) we can use the Born-Oppenheimer (BO) approximation to solve the dimer-wall collision problem. If the heavy particle with mass m_1 is fixed at a distance $x > a/2$ from the wall, the light particle with mass m_2 has a bound state with energy $-\kappa^2(x)/2m_2$, where

$$\kappa(x) = \frac{1}{a} \left[1 + \frac{a}{2x} W \left(-\frac{2x}{a} e^{-\frac{2x}{a}} \right) \right], \quad (31)$$

and W is the Lambert W function. Thus, the heavy particle is governed by an effective single-particle Schrödinger equation:

$$-\frac{1}{2m_1} \frac{d^2\phi(x)}{dx^2} + V_{\text{eff}}(x)\phi(x) = \frac{K^2}{2m_1}\phi(x), \quad (32)$$

where $\phi(0) = 0$ because of the hard wall, and

$$V_{\text{eff}}(x) = \frac{1}{2m_2 a^2} - \frac{\kappa^2(x)}{2m_2} \quad (33)$$

is the effective potential experienced by the heavy particle. In Fig. 1 we show the numerical results for the dimer-wall scattering phase shift δ based on the BO approximation, Eqs. (31), (32) and (33), for the mass ratio $m_1/m_2 = 40$ at $K/K_{\text{th}} \leq 1$, and find good agreement

with the exact numerical results except when K/K_{th} is comparable to 1.

At $x \gg a$,

$$V_{\text{eff}}(x) \approx \frac{1}{m_2 a^2} e^{-2x/a}. \quad (34)$$

For low-energy collisions ($K \ll K_{\text{th}}$) the heavy particle is strongly expelled by the barrier potential $V_{\text{eff}}(x)$, so that $V_{\text{eff}}(x)$ may be approximated by Eq. (34); making this approximation for $V_{\text{eff}}(x)$, we can solve Eq. (32) analytically and find an approximate formula for the dimer-wall scattering phase shift:

$$\delta \approx \frac{\ln 2}{2} K a + \arg \Gamma(1 + i K a) - \frac{K a}{2} \ln \frac{m_1}{m_2}, \quad (35)$$

where $\Gamma(z)$ is the Gamma function. In Fig. 1 we show the predictions of Eq. (35) for $m_1/m_2 = 40$, and find that they are close to our numerical results for the dimer-wall scattering phase shifts at $K \ll K_{\text{th}}$. In Fig. 1 we see that the predictions based on Eqs. (31), (32) and (33) are a better approximation to the exact numerical results for the phase shift than the predictions based on Eq. (35) at $m_1/m_2 = 40$, but that the two approximations are both very close to the exact numerical results for the phase shift at $K/K_{\text{th}} \ll 1$.

Substituting Eq. (35) into the left hand side of Eq. (10) and expanding it in powers of K , we get

$$a_R \approx \frac{1}{2} \left(\ln \frac{m_1}{m_2} + 2\gamma - \ln 2 \right) a, \quad (36)$$

$$r_R \approx \frac{2}{3} a_R \left(1 - C \frac{a^3}{a_R^3} \right), \quad (37)$$

where $\gamma \approx 0.577216$ is Euler's constant, and $C = -\frac{1}{2} \psi^{(2)}(1) \approx 1.20206$. Here $\psi^{(n)}(\xi)$ is the polygamma function of order n . Our numerical results for a_R and r_R approach the BO formulas in Eqs. (36) and (37) at large mass ratios, as shown in Fig. 2.

V. HIGH ENERGY COLLISIONS

For any fixed mass ratio, if K/K_{th} is sufficiently large, the de Broglie wave lengths of the incident particles are very short compared to the size of the dimer, and we can understand the problem semiclassically, assuming that particle 1 has incident velocity v_1 and particle 2 has incident velocity v_2 . Since the magnitude of the center-of-mass velocity of the incident pair is $v_c = K/M$, we have

$$v_1 = -v_c + q/m_1 \quad v_2 = -v_c - q/m_2, \quad (38)$$

where q ($-q$) is the momentum of particle 1 (particle 2) in the center-of-mass frame. The normalized wave

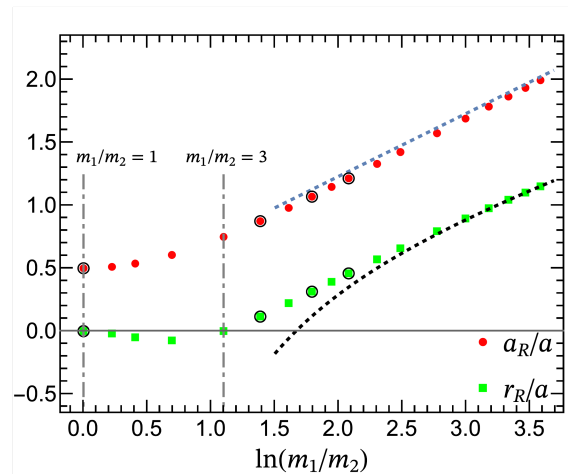


FIG. 2. Dimer-wall scattering length a_R and effective range r_R (in units of the two-body scattering length a) versus the natural logarithm of the mass ratio. The red dots and the green squares show the values of a_R/a and r_R/a , respectively, according to the numerical solution to Eq. (22). The circles are the predictions of Ref. [4]. The blue dashed line shows the prediction of Eq. (36) based on the Born-Oppenheimer (BO) approximation. The black dashed curve shows the prediction of Eq. (37) based on the BO approximation. The vertical dot-dashed lines indicate the integrable cases ($m_1/m_2 = 1$ or 3), for which there are exact results discussed in Sec. II.

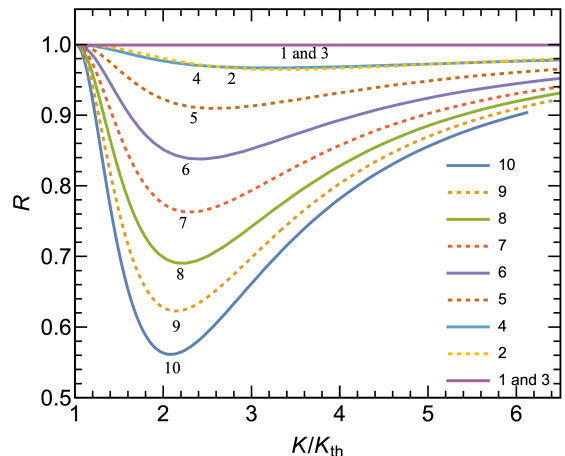


FIG. 3. The reflection coefficient R as functions of K/K_{th} for mass ratios $m_1/m_2 = 1$ to 10. The numbers below the curves are the mass ratios.

function of the dimer in the center-of-mass frame is $\psi_{\text{rel}}(r) = \frac{1}{\sqrt{a}} \exp(-|r|/a)$. The normalized wave function in the momentum representation is thus

$$\tilde{\psi}_{\text{rel}}(q) = \frac{1}{\sqrt{2\pi}} \int_{-\infty}^{\infty} \psi_{\text{rel}}(r) e^{-iqr} dr = \sqrt{\frac{2}{\pi}} \frac{\sqrt{a}}{1 + a^2 q^2}, \quad (39)$$

and the probability of finding the relative momentum in the interval $(q, q + dq)$ is $|\tilde{\psi}_{\text{rel}}(q)|^2 dq$. Since $q \sim 1/a$

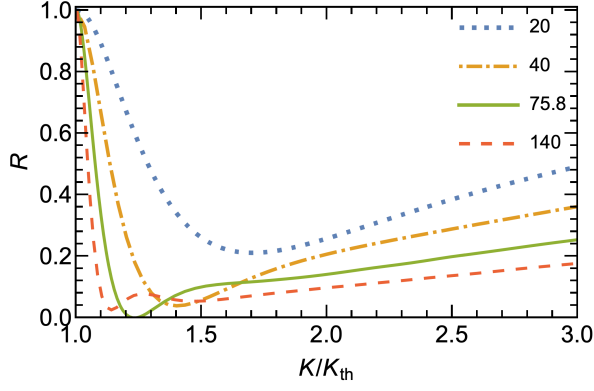


FIG. 4. The reflection coefficient R as functions of K/K_{th} for mass ratios $m_1/m_2 = 20, 40, 75.8$ and 140 . For $m_1/m_2 \approx 75.8$, R reaches zero at $K/K_{\text{th}} \approx 1.24$.

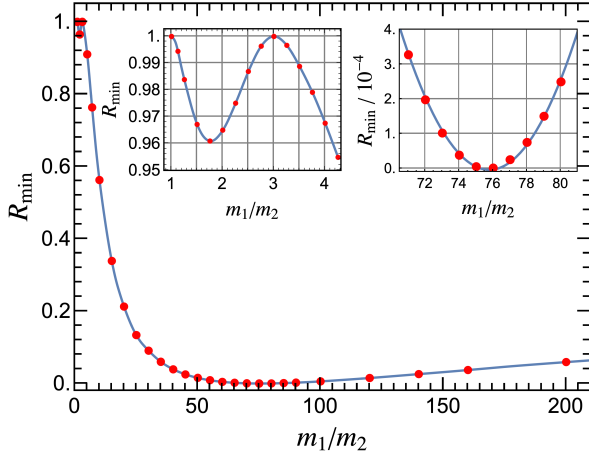
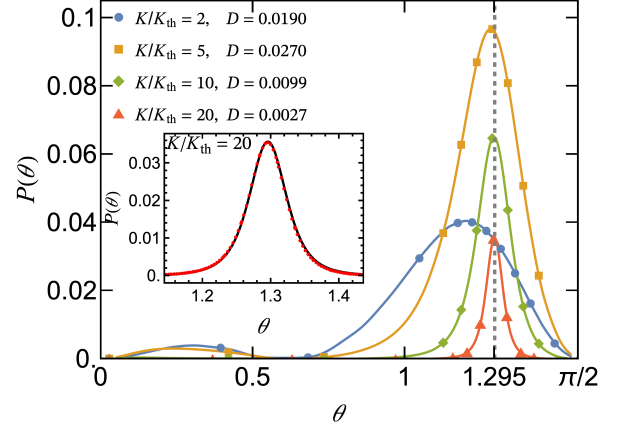


FIG. 5. The minimum value of the reflection coefficient R_{min} for different mass ratios. The left inset plots R_{min} for $1 \leq m_1/m_2 \leq 4.3$. The right inset plots R_{min} for $70.5 \leq m_1/m_2 \leq 81$. We numerically found that $R_{\text{min}} = 0$ at a critical mass ratio $m_1/m_2 \approx 75.8$.

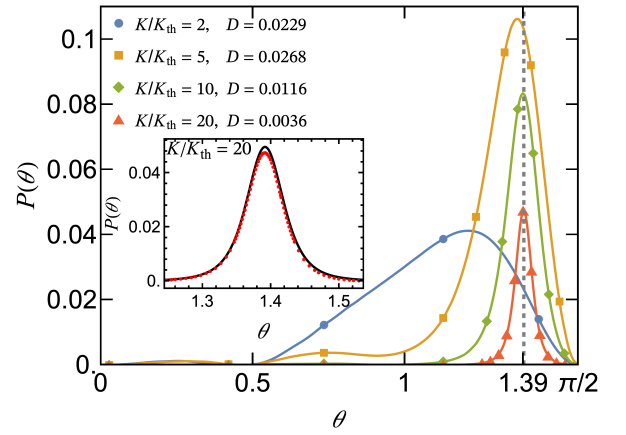
according to this probability distribution, we have $v_1 \approx v_2 \approx -K/M$ at sufficiently large K/K_{th} .

If particle 1 (the heavier particle) is on the left of particle 2 (namely $x_1 < x_2$) before the dimer-wall collision, particle 1 hits the wall first, and its velocity is changed to $-v_1$ after the collision with the wall. Particle 1 then hits particle 2 with relative velocity $v_r \approx 2K/M$, and the probability that they are bounced back from each other is $D_1 = 1/(1 + q'^2 a^2) \approx 1/(q'^2 a^2)$ according to the δ function interaction potential, where $q' = \mu v_r \approx 2m_1 m_2 K/M^2$ is the momentum of particle 1 in the new center-of-mass frame. So $D_1 \approx M^2 K_{\text{th}}^2 / (4m_1 m_2 K^2)$. After the two particles bounce back from each other, particle 1 has a new velocity v'_1 and particle 2 has a new velocity v'_2 satisfying momentum conservation

$$m_1 v'_1 + m_2 v'_2 = -m_1 v_1 + m_2 v_2 \quad (40)$$



(a) $m_1/m_2 = 2$



(b) $m_1/m_2 = 4$

FIG. 6. The “angular distributions” $P(\theta)$ for the dissociated pair for mass ratios 2 (upper graph) and 4 (lower graph) at $K/K_{\text{th}} = 2, 5, 10, 20$. The corresponding values of the dissociation probability D according to Eq. (30) are shown in the graphs. For larger and larger values of K/K_{th} , the curves approach narrower and narrower peaks centered around $\theta = \theta_c$ where θ_c is defined in Eq. (46) and is indicated by a vertical dashed line in each graph. The insets compare the semiclassical results according to Eq. (49) (black solid line) with the exact numerical results (red dots) for $K/K_{\text{th}} = 20$.

and energy conservation

$$\frac{1}{2} m_1 v_1'^2 + \frac{1}{2} m_2 v_2'^2 = \frac{1}{2} m_1 v_1^2 + \frac{1}{2} m_2 v_2^2. \quad (41)$$

Solving the above equations, we get

$$v'_1 = \frac{m_1 - 3m_2}{m_1 + m_2} v_c + \frac{(-3m_1 + m_2)q}{m_1(m_1 + m_2)}, \quad (42)$$

$$v'_2 = \frac{3m_1 - m_2}{m_1 + m_2} v_c + \frac{(m_1 - 3m_2)q}{m_2(m_1 + m_2)}. \quad (43)$$

If $m_1/m_2 < 3$, then for sufficiently large v_c , $v'_1 < 0$, and particle 1 will hit the wall again and its velocity changes to $-v'_1$. In the distant future after the collisions, the coordinates of the particles have a ratio $x_2/x_1 \approx |v'_2|/|v'_1|$ regardless of the mass ratio. Therefore, according to Eq. (26) we have

$$\theta = \arctan\left(\sqrt{\frac{m_2}{m_1}} \frac{|v'_2|}{|v'_1|}\right). \quad (44)$$

At large v_c we may Taylor expand θ to first order in q to find

$$\theta \approx \theta_c + \frac{\sigma}{v_c \sqrt{m_1 m_2}} q, \quad (45)$$

where $\sigma = +1$ if $m_1 > 3m_2$ and $\sigma = -1$ if $m_1 < 3m_2$, and

$$\theta_c = \arctan\left(\left|\frac{3m_1 - m_2}{3m_2 - m_1}\right| \sqrt{\frac{m_2}{m_1}}\right). \quad (46)$$

Therefore, if the dimer breaks up after collision with the wall, the "angle" θ in the distant future has a probability density of approximately $v_c \sqrt{m_1 m_2} |\tilde{\psi}_{\text{rel}}(q)|^2$, and we find

$$D \approx D_1 \approx \frac{(m_1 + m_2)^2}{4m_1 m_2} \frac{K_{\text{th}}^2}{K^2}, \quad (47)$$

and

$$P(\theta) \approx D_1 v_c \sqrt{m_1 m_2} |\tilde{\psi}_{\text{rel}}(q)|^2. \quad (48)$$

Combining Eqs. (39), (45) and (47) with the above equation, we find

$$P(\theta) \approx \frac{(m_1 + m_2)^2 K_{\text{th}}}{2\pi m_1 m_2 K [1 + (K/K_{\text{th}})^2 (\theta - \theta_c)^2]}. \quad (49)$$

If particle 1 (the heavier particle) is on the right of particle 2 before the dimer-wall collision, particle 2 hits the wall first, and its velocity is changed to $-v_2$. Then there is a small probability D_1 that particle 2 is bounced off by particle 1. Then particle 2 hits the wall again, and its velocity gets reversed. Then

- if $m_1 > 3m_2$ particle 2 has nearly 100% probability of passing through particle 1, and then particle 1 hits the wall, and its velocity is reversed;
- if $m_1 < 3m_2$ particle 2 catches up with particle 1 and has nearly 100% probability of passing through particle 1.

One can similarly show that in this case the approximate formulas for D and $P(\theta)$ in Eqs. (47) and (49) remain valid.

Equation (49) shows that $P(\theta)$ peaks at $\theta \approx \theta_c$ and the peak has a narrow width at $K/K_{\text{th}} \gg 1$. In the insets of Fig. 6, we compare the predictions of Eq. (49) with our

numerical results for $P(\theta)$ based on Eqs. (22), (27), and (29), and find excellent agreement when K/K_{th} is large.

In Fig. 7 we plot $(K/K_{\text{th}})^2 D$ [where $D = 1 - R = 1 - |f|^2$ and f is obtained by numerically solving Eqs. (22) and (23)] as functions of K/K_{th} for the mass ratios 2 and 4, and numerically verify the validity of Eq. (47) at large K/K_{th} .

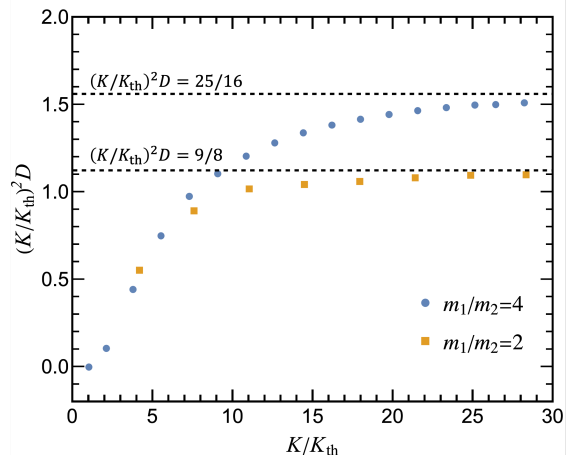


FIG. 7. The scaled dissociation probability $(K/K_{\text{th}})^2 D$ as functions of K/K_{th} for the mass ratios 2 and 4. In the high energy limit, $(K/K_{\text{th}})^2 D$ approaches a constant equal to $\frac{(m_1 + m_2)^2}{4m_1 m_2}$ according to Eq. (47).

VI. SUMMARY

In this work, we have studied the scattering of a dimer from a hard wall in one dimension, assuming a delta function attractive interaction potential between the two constituent particles. We have numerically computed the scattering phase shift and the reflection coefficient as functions of the mass ratio and the collision energy by solving a one-dimensional integral equation. For large mass ratios we used the Born-Oppenheimer approximation to find formulas for the elastic scattering phase shift, the dimer-wall scattering length, and the dimer-wall effective range. For high energy collisions, we used a semi-classical analysis to derive approximate formulas for the dissociation probability and the "angular distribution" of the dissociated pair. For the mass ratio of about 75.8, we find that the reflection coefficient vanishes at a particular collision energy. For the mass ratios of 1 and 3, the problem is integrable and the reflection coefficient is equal to unity for all collision energies.

ACKNOWLEDGMENTS

This work was supported by the National Key R&D Program of China Grant No. 2021YFA1400902, the National Natural Science Foundation of China Grant No.

-
- [1] M. Olshanii, Atomic scattering in the presence of an external confinement and a gas of impenetrable bosons, *Phys. Rev. Lett.* **81**, 938 (1998).
- [2] C. Chin, R. Grimm, P. Julienne, and E. Tiesinga, Feshbach resonances in ultracold gases, *Rev. Mod. Phys.* **82**, 1225 (2010).
- [3] S. Montangero, D. Frustaglia, T. Calarco, and R. Fazio, Quantum billiards in optical lattices, *EPL (Europhysics Letters)* **88**, 30006 (2009).
- [4] D. Lee and M. Pine, How quantum bound states bounce and the structure it reveals, *The European Physical Journal A* **47**, 10.1140/epja/i2011-11041-4 (2011).
- [5] A. L. Gaunt, T. F. Schmidutz, I. Gotlibovych, R. P. Smith, and Z. Hadzibabic, Bose-einstein condensation of atoms in a uniform potential, *Phys. Rev. Lett.* **110**, 200406 (2013).
- [6] J. J. P. van Es, P. Wicke, A. H. van Amerongen, C. Rétif, S. Whitlock, and N. J. van Druten, Box traps on an atom chip for one-dimensional quantum gases, *Journal of Physics B: Atomic, Molecular and Optical Physics* **43**, 155002 (2010).
- [7] T. F. Schmidutz, I. Gotlibovych, A. L. Gaunt, R. P. Smith, N. Navon, and Z. Hadzibabic, Quantum joule-thomson effect in a saturated homogeneous bose gas, *Phys. Rev. Lett.* **112**, 040403 (2014).
- [8] B. Mukherjee, Z. Yan, P. B. Patel, Z. Hadzibabic, T. Yefsah, J. Struck, and M. W. Zwierlein, Homogeneous atomic fermi gases, *Phys. Rev. Lett.* **118**, 123401 (2017).
- [9] K. Hueck, N. Luick, L. Sobirey, J. Siegl, T. Lompe, and H. Moritz, Two-dimensional homogeneous fermi gases, *Phys. Rev. Lett.* **120**, 060402 (2018).
- [10] M. Olshanii and S. G. Jackson, An exactly solvable quantum four-body problem associated with the symmetries of an octacube, *New Journal of Physics* **17**, 105005 (2015), publisher: IOP Publishing.
- [11] B. Parajuli, D. Pećak, and C.-C. Chien, Mass-imbalance-induced structures of binary atomic mixtures in box potentials, *Phys. Rev. A* **100**, 063623 (2019).
- [12] Y. Liu, F. Qi, Y. Zhang, and S. Chen, Mass-imbalanced atoms in a hard-wall trap: An exactly solvable model associated with d6 symmetry, *iScience* **22**, 181 (2019).
- [13] L. Anderegg, L. W. Cheuk, Y. Bao, S. Burchesky, W. Ketterle, K.-K. Ni, and J. M. Doyle, An optical tweezer array of ultracold molecules, *Science* **365**, 1156–1158 (2019).
- [14] L. W. Cheuk, L. Anderegg, Y. Bao, S. Burchesky, S. S. Yu, W. Ketterle, K.-K. Ni, and J. M. Doyle, Observation of collisions between two ultracold ground-state caesium molecules, *Phys. Rev. Lett.* **125**, 043401 (2020).
- [15] W. B. Cairncross, J. T. Zhang, L. R. B. Picard, Y. Yu, K. Wang, and K.-K. Ni, Assembly of a rovibrational ground state molecule in an optical tweezer, *Phys. Rev. Lett.* **126**, 123402 (2021).
- [16] L. R. Liu, J. D. Hood, Y. Yu, J. T. Zhang, N. R. Hutzler, T. Rosenband, and K.-K. Ni, Building one molecule from a reservoir of two atoms, *Science* **360**, 900–903 (2018).
- [17] W.-L. Li, H.-J. Song, T.-L. Song, and D. Zhou, Dissociation of a one-dimensional cold molecule via quantum scattering, *Communications in Theoretical Physics* **75** (2023).
- [18] A. M. Moro, J. A. Caballero, and J. Gomez-Camacho, One dimensional scattering of a two body interacting system by an infinite wall (2010), [arXiv:1010.4933 \[nucl-th\]](https://arxiv.org/abs/1010.4933).
- [19] J. P. Gomez, A. Minguzzi, and M. Olshanii, Traces of integrability in scattering of one-dimensional dimers on a barrier, *New Journal of Physics* **21**, 023008 (2019).
- [20] C. Baroni, G. Lamporesi, and M. Zaccanti, Quantum mixtures of ultracold gases of neutral atoms, *Nature Reviews Physics* **6**, 736 (2024).
- [21] E. Wille, F. M. Spiegelhalter, G. Kerner, D. Naik, A. Trenkwalder, G. Hendl, F. Schreck, R. Grimm, T. G. Tiecke, J. T. M. Walraven, S. J. J. M. F. Kokkelmans, E. Tiesinga, and P. S. Julienne, Exploring an ultracold fermi-fermi mixture: Interspecies feshbach resonances and scattering properties of ^6Li and ^{40}K , *Phys. Rev. Lett.* **100**, 053201 (2008).
- [22] A.-C. Voigt, M. Taglieber, L. Costa, T. Aoki, W. Wieser, T. W. Hänsch, and K. Dieckmann, Ultracold heteronuclear fermi-fermi molecules, *Phys. Rev. Lett.* **102**, 020405 (2009).
- [23] L. Costa, J. Brachmann, A.-C. Voigt, C. Hahn, M. Taglieber, T. W. Hänsch, and K. Dieckmann, *s*-wave interaction in a two-species fermi-fermi mixture at a narrow feshbach resonance, *Phys. Rev. Lett.* **105**, 123201 (2010).
- [24] H. Hara, Y. Takasu, Y. Yamaoka, J. M. Doyle, and Y. Takahashi, Quantum degenerate mixtures of alkali and alkaline-earth-like atoms, *Phys. Rev. Lett.* **106**, 205304 (2011).
- [25] A. Green, H. Li, J. H. See Toh, X. Tang, K. C. McCormick, M. Li, E. Tiesinga, S. Kotochigova, and S. Gupta, Feshbach resonances in *p*-wave three-body recombination within fermi-fermi mixtures of open-shell ^6Li and closed-shell ^{173}Yb atoms, *Phys. Rev. X* **10**, 031037 (2020).
- [26] L. J. LeBlanc and J. H. Thywissen, Species-specific optical lattices, *Phys. Rev. A* **75**, 053612 (2007).
- [27] M. Gaudin, Boundary energy of a bose gas in one dimension, *Phys. Rev. A* **4**, 386 (1971).
- [28] L. Dodd, Numerical study of a model three-body system, *Australian Journal of Physics* **25**, 507 (1972).
- [29] V. A. Yurovsky, A. Ben-Reuven, and M. Olshanii, One-dimensional bose chemistry: Effects of nonintegrability, *Phys. Rev. Lett.* **96**, 163201 (2006).
- [30] N. L. Harshman, One-Dimensional Traps, Two-Body Interactions, Few-Body Symmetries: I. One, Two, and Three Particles, *Few-Body Systems* **57**, 11 (2016).
- [31] N. L. Harshman, Infinite barriers and symmetries for a few trapped particles in one dimension, *Phys. Rev. A* **95**, 053616 (2017).